Compositional and structural characterization of silicon nanoparticles embedded in silicon rich oxide

J.A. Luna-López, M. Aceves-Mijares, O. Malik, and Z. Yu
Instituto Nacional de Astrofísica, Óptica y Electrónica, INAOE, Puebla 72000, México,
e-mail: jluna@inaoep.mx, maceves@ieee.org, amalik@inaoep.mx

A. Morales and C. Domínguez
IMB–CNM, CSIC. Campus UAB. 08193 Bellaterra, España.

J. Rickards
Instituto de Física, Universidad Nacional Autónoma de México,
Apartado Postal 20-364, Mexico D.F.

Recibido el 30 de noviembre de 2006; aceptado el 8 de octubre de 2007

Silicon Rich Oxide (SRO) is a dielectric material that contains Si nanoparticles, thus showing novel physical characteristics which permits its use in optoelectronic devices. In this work, the composition and structure at the surface, volume and Si/SRO interface of the SRO films deposited on c-Si substrates were studied. Different techniques, such as Atomic Force Microscopy (AFM), High Resolution Transmission Electronic Microscopy (HRTEM), Rutherford Backscattering Spectrometry (RBS) and X-ray Photoelectron Spectroscopy (XPS) were used in the study. XPS and RBS reveal that the composition of the films varied with respect to the gas flow ratio. These results allow us to correlate the compositional and structural [as size of the grains (roughness), nc-Si size and different oxidation states of Si] changes of the surface, volume and interface from the SRO films with the flow ratio (Ro) used during the deposition process and with the high temperature annealing time.

Keywords: Silicon rich oxide; AFM; HRTEM; nanocrystals; surface roughness; RBS; XPS.

El óxido de silicio rico en silicio (SRO) es un material dieléctrico que contiene nanopartículas de silicio. Por lo tanto muestra características físicas novedosas las cuales permiten su uso en dispositivos opto electrónicos. En este trabajo, fueron estudiadas la composición y estructura de la superficie, volumen e interfaz del SRO/Si de las películas de SRO depositadas sobre substrato de silicio. En este estudio fueron usadas diferentes técnicas como Microscopia de fuerza atómica (AFM), Microscopía electrónica de transmisión de alta resolución (HRTEM), Espectroscopia de retrodispersión de iones Rutherford (RBS) y Espectroscopia de fotoelectrones de rayos-X (XPS). XPS y RBS revelan que la composición de las películas varía con respecto a la Ro. Estos resultados nos permiten relacionar los cambios estructurales y composicionales [como el tamaño de grano (Rugosidad), tamaño de los nanocristales de silicio, y de los diferentes estados de oxidación del silicio] de la superficie, volumen e interfaz de las películas de SRO con la razón de flujo Ro y tiempo de tratamiento térmico.

Descriptores: Óxido de silicio rico en silicio; AFM; HRTEM; nanocristales; rugosidad superficial; RBS; XPS.

PACS: 73.22.-f; 79.20.Rf; 81.07.Bc; 82.80.Pv

1. Introduction

Silicon Rich Oxide (SRO) thin films have been intensively studied because of their technological importance for optoelectronic devices based on silicon technology. To date, the atomic structures of the films and their physical properties, such as the optical and electrical characteristics, have not yet been fully understood. SRO can be considered as a multiphase material composed of a mixture of stoichiometric silicon oxide (SiO_2), off stoichiometric oxide (SiO_x, x<2) and elemental silicon (as nanocrystals). SRO can be prepared by a number of techniques including silicon ion implantation into the thermal dioxide films [1], reactive sputtering [2], co-evaporation [3], sol-gel, low pressure chemical vapor deposition (LPCVD) [4] and plasma enhanced chemical vapor deposition (PECVD) [5]. In all of these techniques, the silicon excess can be controlled by changing the process parameters. Thermal treatments are generally used to enhance the luminescent properties of the SRO films. Depending on the precursor gas flow ratio (Ro) and thermal annealing time, it is possible to obtain Si-nc's and nanodots <10 nm and ≤ 1 nm in size, respectively. In this work, we will present our experimental results on the characterization of surface, volume and interface structure of SRO films. The morphology of SRO has been determined by AFM. AFM images show different morphologies at the surface of the SRO films depending on the flow ratio (Ro) and thermal treatment time; because the annealing process caused the grain agglomeration. All images show grain like structure with nanometer size, which was characterized by height distribution, average roughness and grain and pore average diameter. The composition was obtained by RBS and XPS techniques; the results show a SiO_2 small layer formed at the surface of the SRO films. The composition of the SRO films and oxidation states in the surface, volume and interfaces varied with the flow ratio, Ro. The size of the silicon nanocrystals was obtained by HRTEM, and it has been found that the size varied in agreement with the flow ratio and thermal treatment time.

2. Experiment

SRO films were deposited on N type Silicon (100) substrates with a resistivity of 2-5 Ω-cm. SRO layers were obtained in a horizontal LPCVD hot wall reactor using SiH_4 (Silane) and N_2O (nitrous oxide) as reactive gases at 700°C. The gas flow ratio, Ro = $[N_2O]/[SiH_4]$ = 10, 20 and 30, was used to control the amount of excess silicon in the SRO films, and the pressure was varied for each Ro from 1.64- 1.94 Torr. After deposition, the samples were densified by a thermal annealing at 1000°C in N_2 during 30 minutes. Some of the densified samples were also thermally annealed at 1100 °C in N_2 during 180 minutes. The surface morphologies of SRO samples were studied using an easyScan Dynamic Force Microscope (DFM) Nanosurf system version 2.3, operating in a static mode. The topography for each image was measured at a scan size of 4×4 μm^2. For each sample, several different scans were done with good reproducibility. The AFM images were statistically analyzed with the software Scanning Probe Image Processor (SPIP). Average roughness and grain and pores diameter were calculated from AFM images. The sizes of the nc-Si were obtained using Tencai F30 high resolution transmission electron microscope (HRTEM) operated with an acceleration voltage of 300 kV. The oxygen and silicon content of the as deposited SRO films was obtained by RBS of 3.2 MeV α-particles beam of 1 mm diameter; the α-particles were obtained using the 3MV 9SDH-2 Pelletron accelerator, and projectiles scattered at 168° were detected with an OXFORD 50-11 surface barrier detector. XPS data were obtained using a PHI ESCA-5500 X-ray photoelectron spectrometer with an Al radiation, E = 1486 eV.

3. Results

In this section, we show the results obtained from the different techniques used. RBS spectra of the as deposited SRO films are shown in Fig. 1. It shows two different profiles corresponding to Ro = 20 and 30; the other two profiles are the respective simulations in order to analyze the RBS spectra and to find the oxygen and silicon content in the films, which were done using the software SIMRA version 5.02 [6].

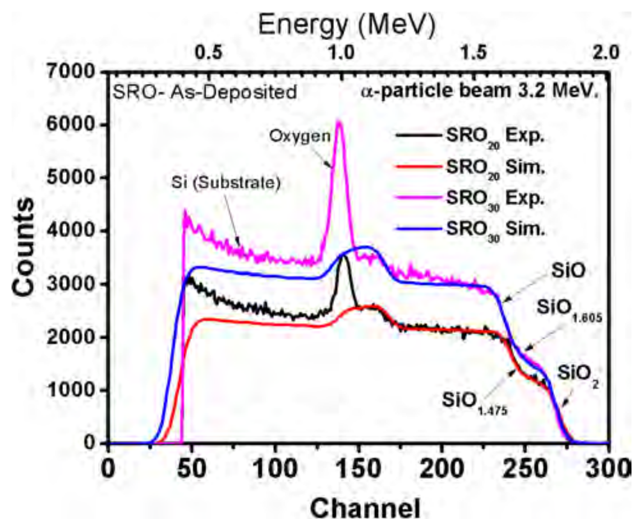

FIGURE 1. SRO films RBS Spectra. The samples were deposited with a flow ratio Ro = 20 and 30. Experimental (Exp.) curves were compared with simulated (Sim.) curves.

TABLE I. Compositional results of SRO films obtained by XPS.

Ro	Thickness	Concentration			Si Excess	x = O/Si
	nm	O%	Si%	N or Ar%	%	
10	100.00	53.50	45.50	1.00	12.50	1.176
20	655.10	60.81	38.46	0.73	5.46	1.580
30	696.60	62.01	37.35	0.64	4.35	1.660

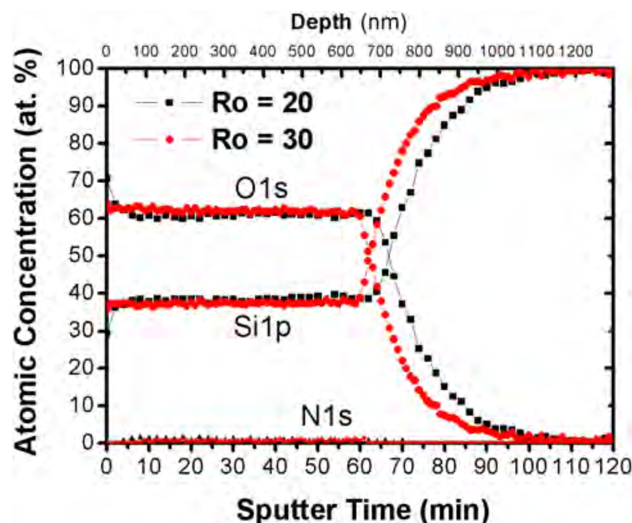

FIGURE 2. XPS spectra show the composition of the SRO films, for Ro = 20 and 30.

In both films, a small layer of SiO_2 was found in the surface. In the SRO bulk, the silicon and oxygen ratio was determined to be 0.43/0.57 and 0.37/0.62 for Ro = 20 and Ro = 30, respectively. The layer thickness was found by RBS to be ≈ 490 nm, and the superficial layer of SiO_2 is ≈ 10 nm for both samples. The simulation was established supposing different SiO_2, SiO_x, SiO layers, until the better approximation was obtained. Figure 2 shows the composition of the SRO films obtained by XPS. Figure 2 corresponds to Ro = 20 and 30. In Table I are listed the composition results of the XPS spectra.

Figure 3 shows XPS experimental spectra of the Si $2p$ line and the evolution of the Si $2p$ line in the surface, volume and interface SRO/Si. Figure 3 corresponds to Ro = 10. The four oxidation states, as well as the unoxidized state, can be modelled as tetrahedral bonding units, in which a central Si atom is bonded to (4-n) Si atoms and n oxygen atoms ($Si\text{-}Si_{4-n}O_n$) with n = 0 to 4. Therefore, the 99.2 eV peak is associated to elemental silicon. SiO_2 spectra increases the peak energy to 103.6 eV, corresponding to n=4. In the case of the Ro = 10, the shift in the peak position is due to a charge effect. The Si 2p binding energies are about 98 to 104 eV. The cause of the shifts in the peak position is due to the variation

of the oxidation states of the SRO films. In Ro = 10, a peak at about 100.7 eV, in some cases accompanied by a peak at about 103.6 eV, are present; they can be attributed to Si and SiO_2, respectively, and any variation could be attributed to sub oxidized silicon [7,8].

The increasing electronegativity of the Si-O bound relative to the Si-Si bond results in a shift to a higher binding energy of the core level electrons in the silicon.

It is widely accepted that the Si 2p photoelectron peak of SiO_x contains five components, corresponding to a non oxidized state and four different oxidation states of Si [9,10].

The AFM images of SRO films a) as deposited, b) thermally annealed at 1100 °C for 180 minutes are presented in Fig. 4. It can be seen that the surface exhibits different characteristics depending on the Ro, which influence the size of the grains (roughness), their form and composition. The average roughness $\langle Sa \rangle$ measured for Ro = 10, 20 and 30 as deposited was 17, 10 and 8 nm, respectively. Average roughness is the highest for Ro = 10 and decreases for Ro = 20 and 30 after thermal treatments, which is probably due to the agglomeration of the Si nanocrystals in Ro = 10 [8]. On the other hand, the structure of SRO films was analyzed using an HRTEM. Figure 5 shows the HRTEM images for the SRO films with thermal annealing at 1100 °C for 180 minutes. Figure 5a indicates the presence of silicon agglomerates forming nc-Si in the SRO film with 12.5 at.% of silicon excess. Some of them are semi-elliptical, and some others have an enlarged shape. The agglomeration process takes place between the nearest Si-nanoclusters forming nc-Si. A great dispersion of diameter sizes is observed; the diameter size goes from 3 up to 9 nm, being the average diameter size around 5.7 nm, as indicated in the histogram. Fig. 5b shows the HRTEM image for the SRO film with 5.46 at.% of silicon excess. Si-nanoclusters are also observed in this film. The image exhibits Si-clusters uniformly distributed in the SRO film. Si-nanoclusters diameter sizes are extended from 1.5 to 4 nm, with an average diameter size of 2.7 nm, and with spherical shape. Si-nanoclusters were not observed in the SRO film after annealing at 1100°C with 4.35 at.% of silicon excess. The existence of Si-nanoclusters with a size < 1nm is possible, but not resolved in the images.

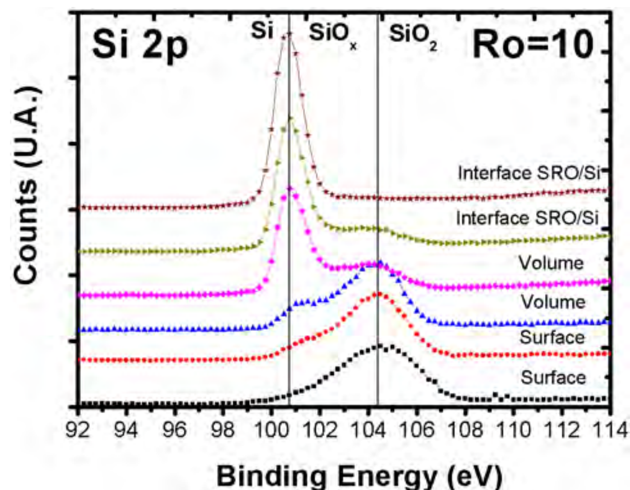

FIGURE 3. Si 2p XPS spectra at a different position inside the SRO layer, in the surface, volume and interface of the film SRO_{10}.

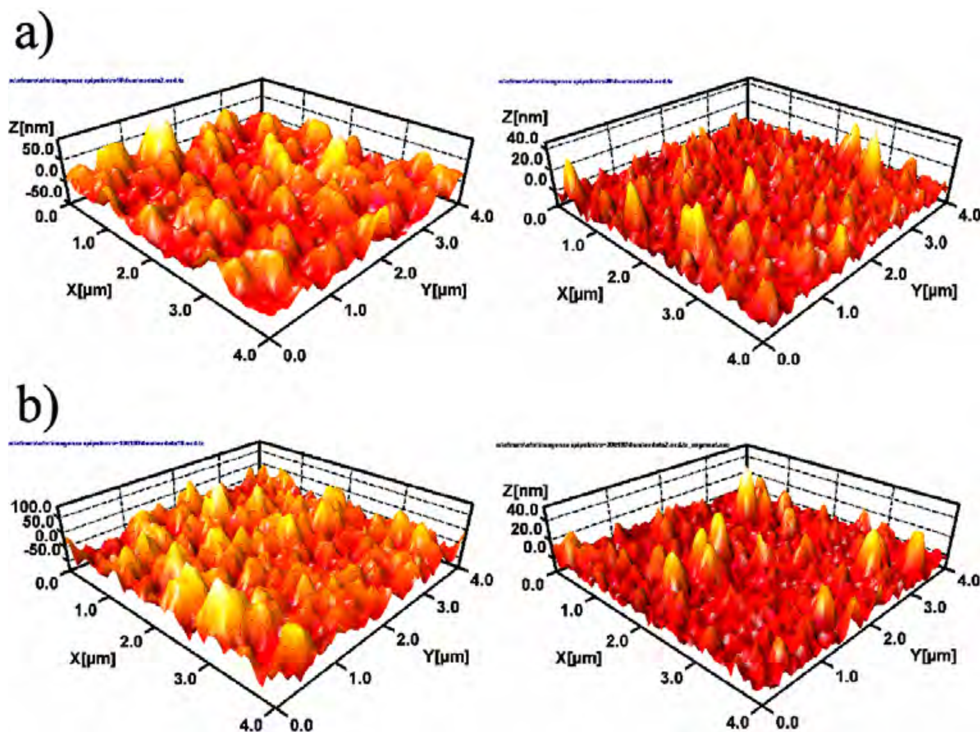

FIGURE 4. Comparison AFM images in 3-D from SRO_{10} and SRO_{30} films a) without and b) with thermal annealing, with a size scanner of $4 \times 4\ \mu m^2$.

TABLE II. Oxidation states of the SRO films obtained by means of the convolution of the XPS curves.

Ro	Location in the Films	Oxidation States Peak position (eV)				
		Si^0	Si^{1+}	Si^{2+}	Si^{3+}	Si^{4+}
10	Surface				103.60	104.78
	Volume	100.70	101.70	102.97		104.10
	Interface SRO/Si	99.65 100.71				
20	Surface			102.50	103.45	105.50
	Volume			102.10	103.90	106.00
	Interface SRO/Si	100.76		102.00	103.88	
30	Surface		101.57		103.81	105.00
	Volume			102.54		104.42
	Interface SRO/Si			102.38		104.11

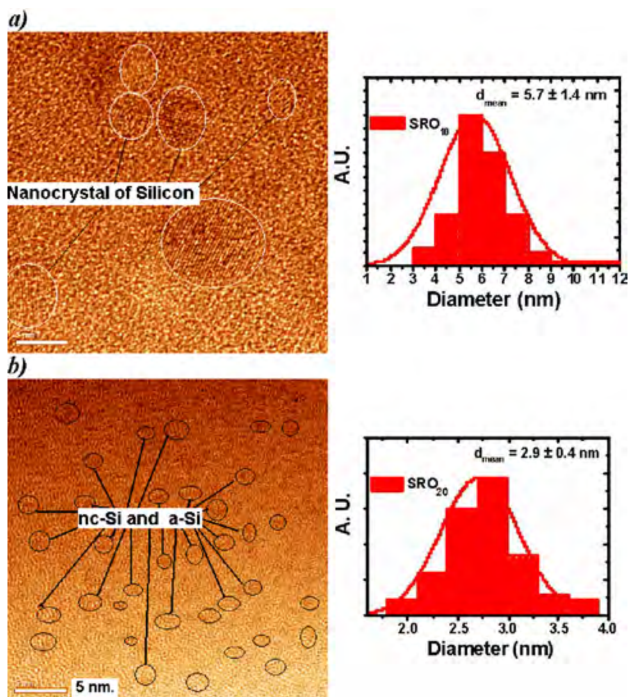

FIGURE 5. HRTEM images and size distribution of nc-Si for the SRO film on both images, the scale is 5 nm, with a) 12.5 at. % and b) 5.46 at.% of silicon excess, and annealed at 1100°C for 180 minutes.

4. Analysis and discussion

The Si concentration of the SiO_x (x≤2) films has been obtained from RBS and XPS measurements. From the XPS measurements, we have different states of oxidation in the films for Ro = 10. As it can be seen in the spectrum of Fig. 3 in the surface, a peak corresponding to SiO_2 is observed. In the volume, the peak position shifts towards SiO_2, indicative of phase separation, and the peak width increases; then, a deconvolution was done, and four peaks around 100.7, 101.7, 102.97 and 104.6 eV were obtained for Ro = 10. Each peak was attributed to Si^0, Si^{1+}, Si^{2+}, and Si^{4+} respectively. The peak position at 100.7 eV is elemental silicon and 104.6 is SiO_2 [9, 10]. In the interface SRO/Si we have two peaks at 99.65 eV and 100.7 eV; again, the first and second are attributed to elemental Si (Si^0). This variation is due to the fact that in the interface there is more silicon, and the position of this peak varied from 99 at 101 eV. In HRTEM, nc-Si were observed for SRO films with Ro = 10. Then, by means of the XPS and HRTEM, it is possible to confirm the formation of the nc-Si. For Ro = 20 and 30, the behavior of the curves XPS are similar in the surface, volume and interface. In the surface, a small layer of SiO_2 is formed, which is represented by a peak at 103.6 eV. In the volume and interface, the peaks are near to 104.4 eV. Also, the elemental silicon peak is weak or vanishes. These results are listed in Table III. These two facts indicate the lack of formation of Si nanoclusters in these films. The shifting of the Si 2p spectra is due to the oxidation states of silicon; in this case, there is no phase separation probably due to less silicon excess in the films,. This result agrees with the results of HRTEM for Ro = 30, in which Si nanoclusters weren't observed.

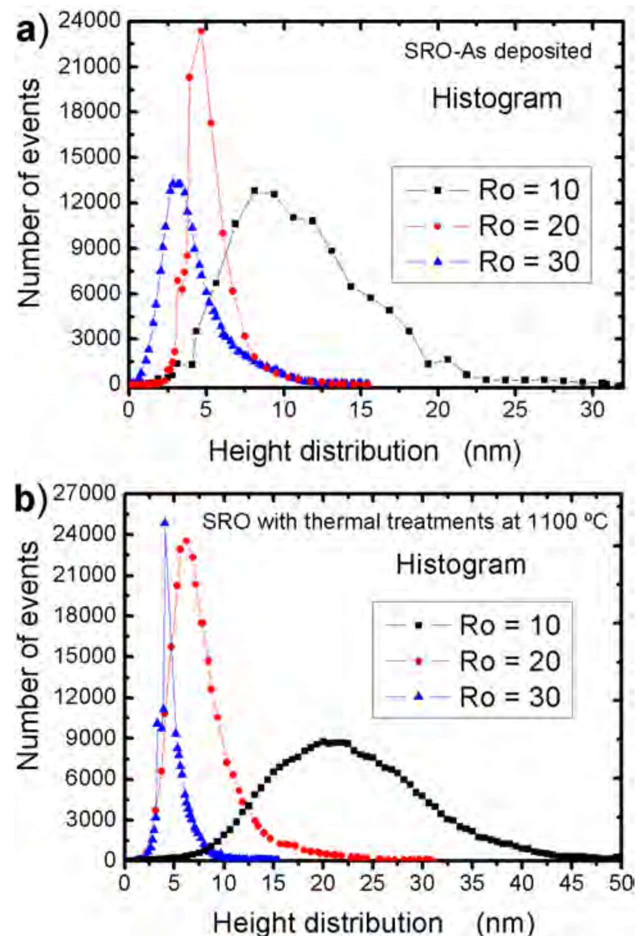

FIGURE 6. Peaks' height distribution of the SRO films for a scanned area of 4×4 μm^2 obtained by AFM. Each graph was classified as: a) SRO films as deposited, b) SRO films with thermal treatments at 1100°C.

TABLE III. Statistic results of AFM obtained for SRO films.

Parameter	Average Roughness $\langle Sa \rangle$ (nm)			Grain Diameter $\langle G \rangle$ (nm)			Pores Diameter $\langle P \rangle$ (nm)		
Flow Ratio (Ro)	10	20	30	10	20	30	10	20	30
As deposited	17	10	8	514	270	206	273	232	132
Densificated at 1000 °C	22	7	7	330	224	331	306	176	158
Annealed at 1100 °C	24	6	5	243	83	167	211	88	129

SRO surface morphology was studied with AFM as a function of the Ro and annealing. The shape of the grain and size in the surface of the SRO films changes with the flow ratio Ro. In the films, the surface roughness decreases notably when the silicon excess reduces (17, 9 and 5 nm for Ro = 10, 20 and 30, respectively), in films as deposited, densified at 1000 °C, and annealed at 1100°C; the roughness increases in SRO_{10} to 17, 22 and 24 nm, respectively. But for SRO_{20}, the roughness decreases to 10, 7 and 6 nm, respectively; and for SRO_{30}, it also decreases to 8, 7, 5 nm ,respectively, as shown in Table III. Fig. 6 shows the height distribution of the roughness for the three Ro's; it confirms that the roughness reduces as Ro increases. The height of the peaks is bigger in SRO_{10} than in SRO_{20} and SRO_{30}, and varied with the thermal annealing. SRO_{20} and SRO_{30} seem to have the same height. In this case, it is probable that the AFM measurement are limited to the size of the tip.

Due to this uncertainty in SRO_{20} and SRO_{30}, the discussion will be centered on the extremes: Ro=10 and 30. As can be seen in Fig. 6a, the average height of the peaks is bigger for SRO_{10}, but the change for SRO_{20} and SRO_{30} is almost not noticeable. From HRTEM studies, it has been observed that for SRO_{10}, the thermal annealing at 1100°C produces agglomeration of Si, which probably formed nc-Si by diffusion [8].

Then, the growth of the peaks in SRO_{10} is related to the growth of the nc-Si. However, for SRO_{30} the Si does not agglomerate, as discussed before for the HRTEM and XPS results. Then, it is possible that the defects dominate in the SRO_{30} film, rather than nc-Si. In Table 3 are listed the mean values of roughness $\langle Sa \rangle$, grain diameter $\langle G \rangle$ and pore diameter $\langle P \rangle$ as a function of Ro and thermal treatments. The $\langle Sa \rangle$, $\langle G \rangle$ and $\langle P \rangle$ are bigger for SRO_{10} than for SRO_{20} and SRO_{30} and varied with the annealing.

In this case, the threshold detection method was used to obtain $\langle G \rangle$ and $\langle P \rangle$. Only the part of the segment above the threshold is considered a Grain, while the rest is disregarded. Alternatively, the segment parts under the threshold level are the Pores. In the Pore mode, only pixels under the detection level are considered. The detection and statistical analysis of the Grains/Pores was done using the SPIP Program [11].

5. Conclusion

In conclusion, RBS, XPS, HRTEM and AFM were all able to measure compositional and structural differences between SRO films with different silicon excess which varied with the gas flow ratio Ro and thermal treatments. RBS and XPS allow seeing the differences on the SRO surface in the bulk and in the interface as oxidation states and concentration, which depend on the Ro. HRTEM and XPS confirmed the existence of the nc-Si in the volume and interface to SRO_{10}. The films consisted of three phases: Si-Si, SiO_x and SiO_2, depending on the Ro. AFM was able to analyze the surface morphology of SRO films, where the height, roughness and mean diameter of the grain and pores have a significant change with respect to the flow ratio and different annealing time.

Acknowledgment

We would like to thank CONACYT for support granted through scholarship # 145068 and CONCYTEP-FOMIX for providing support to this work. The authors also thank Pablo Alarcón, Mauro Landa, Carlos Zúñiga, Ignacio Juárez and Netzhualcoyotl Carlos for helping in the preparation of the samples, and R. Trejo-Luna, K. López, F. Jaimes and A. Heredia for helping in the experiment of RBS.

1. L. Pavesi, L. Dal Negro, L. Mazzoleni, G. Franzo, and F. Priolo, *Nature* **408** (2000) 440.
2. O. Hanaizumi, K. Ono, and Y. Ogawa, *Appl. Phys. Lett.* **82** (2003) 538.
3. Y.C. Fang *et al.*, *Nanotechnology* **15** (2004) 495.
4. D. Dong *et al.*, *J. Electrochem. Soc.* **125** (1978) 819.
5. P.G. Pai, S.S. Chao, and Y. Takagi, *J. Vac. Sci. Technol. A* **4** 689 (1986).
6. Mayer Matej, Software SIMNRA versión 5.02, Max Plank -Institute für Plasmaphysik, D-85748 Garching, Germany, 1997-2004.
7. F. Iacona, G. Franzo, and C. Spinella, *J. Appl. Phys.* **87** (2000) 1295.
8. F. Iacona, C. Borgiono, and C. Spinella, *J. Appl. Phys.* **95** (2004) 3723.
9. Shinji Hayashi, Shinichi Tanimoto, and Keiichi Yamamoto, *J. Appl. Phys.* **68** (1990) 5300.

10. L.B. Mag, A.L. Ji, C. Liu, Y.Q. Wang, and Z.X. Cao, *J. Vac. Sci. Technol. B* **22** (2004) 2654.
11. The Scanning Probe Image Processor (SPIP), image metrology www.imagemet.com., 2005.